Check for updates

1310 Vol. 42, No. 6 / June 2025 / *Journal of the Optical Society of America B* **Research Article**

Journal of the Optical Society of America B

OPTICAL PHYSICS

Semiclassical calculation of the power saturation of the Kerr effect in Rb vapor. II: the effect of incomplete optical pumping

ZACHARY H. LEVINE

Quantum Measurement Division, National Institute of Standards and Technology, Gaithersburg, Maryland 20899-8410, USA (zlevine@nist.gov)

Received 20 December 2024; revised 7 April 2025; accepted 24 April 2025; posted 24 April 2025; published 21 May 2025

Rubidium vapor cells play a key role in contemporary quantum optics since they have strong nonlinear interactions with a low-power incident laser light. The simplest nonlinear interaction is the Kerr effect. Although most calculations concentrate on the unsaturated Kerr effect, the saturated Kerr effect has been measured in many materials including ^{85}Rb and ^{87}Rb vapor. Moreover, entanglement-generating vapor cells often operate in the saturated regime. Here, the calculation of the saturated Kerr effect for rubidium vapor at the D2 line uses a density matrix formulation that includes two hyperfine-split levels and all magnetic sublevels in each of the ground and excited states to account for incomplete optical pumping: the transit time of the atoms through the beam is too short to reach a final population distribution. The calculation shows a rapid qualitative change at low optical power, in semiquantitative agreement with experimental data.

https://doi.org/10.1364/JOSAB.553632

1. INTRODUCTION

Nonlinear optical interactions are at the heart of quantum optics [1,2], including phenomena such as entangled photon generation via parametric down-conversion [3], electromagnetically induced transparency [4], stimulated Raman adiabatic passage (STIRAP) [5], and ultrafast pulse generation [6]. Rubidium vapor cells in particular play an important role in quantum optics [7,8] including a compact, accurate clock [9].

The Kerr effect may be most fundamental of all nonlinear processes since it involves one beam at a single frequency and occurs in all media. In the usual formulation, the index of refraction obeys

$$n(I) = n_0 + n_2^{(u)} I, \tag{1}$$

where n_0 is the linear index of refraction, $n_2^{(u)}$ is the unsaturated Kerr coefficient, I is the optical intensity, and $n(I)$ is the intensity-dependent index of refraction. Both n_0 and $n_2^{(u)}$ have complex numerical values which are independent of the intensity. While this works well in many cases, there are numerous exceptions [10]. In particular, it is relatively easy to saturate the Kerr effect in a rubidium vapor cell with a moderate laser power [11].

In saturation, the Kerr coefficient depends on the optical intensity I via the relation

$$n(I) = n_0 + n_2^{(s)}(I) I, \tag{2}$$

introducing the saturated Kerr coefficient $n_2^{(s)}(I)$. The term "saturated" is used because typically $|n_2^{(s)}(I)|$ is monotonically decreasing with I. As always, $n^2 = 1 + \chi$, where χ is the susceptibility. If $\chi \ll 1$, which is typical of atomic vapor systems, then to a good approximation

$$n_2^{(s)} = \frac{\chi - \chi^{(1)}}{2I}, \tag{3}$$

where $\chi^{(1)}$ is the low-field susceptibility and χ is a function of the optical intensity I.

The saturated susceptibility is not usually studied theoretically. The prevailing method has been to measure in the saturated regime and extrapolate to the unsaturated regime for a comparison to theory [11]. The formula for the unsaturated Kerr coefficient used in Ref. [11] may be obtained from a Taylor expansion of the susceptibility for a two-level system [12]. In the first paper of this series, there is a direct comparison of the saturated Kerr coefficient and the two-level system [13]. While it showed reasonable agreement with the data for larger optical power, the two-level theory did not capture the rapid variation of the Kerr coefficient at low power. This might be counterintuitive given that the low-field limit corresponds most closely to the unsaturated Kerr coefficient.

Our collective intuition is based on textbook arguments, such as the derivation of Fermi's Golden Rule, which rely on the system being exposed to light for a very long time. Most relevant here, the susceptibility formula for the two-level system corresponds to the limit of long exposure to the laser field [12]. However, under the experimental conditions of McCormick

0740-3224/25/061310-05 Journal © 2025 Optica Publishing Group

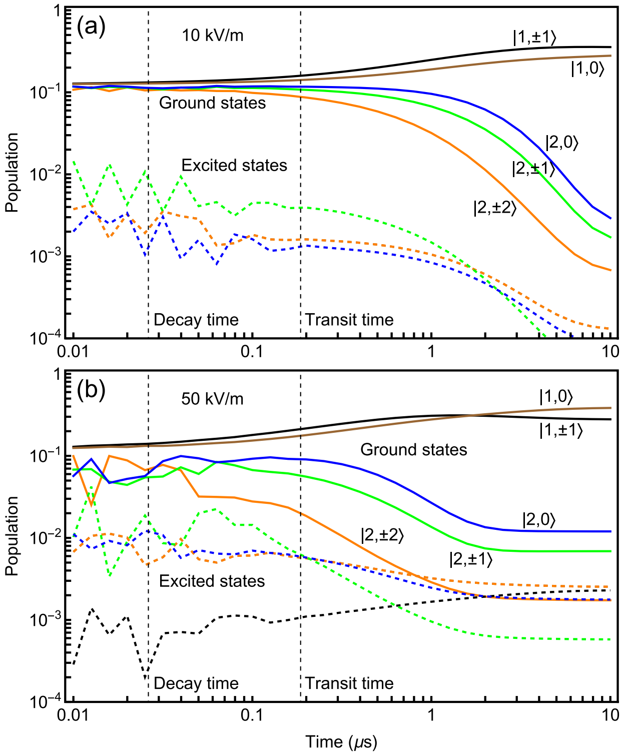

Fig. 1. Calculated populations of ^{87}Rb as a function of time for atoms with equal initial populations in the ground state under optical pumping with a red detuning $\Delta = -0.5$ GHz with a π-polarized electric field of (a) 10 kV/m and (b) 50 kV/m. Under π polarization, the populations are symmetric in the sign of the magnetic quantum number. The populations of the ground and excited states are shown with solid and dashed lines, respectively. The decay time [15] and the mean transit time, given in Section 2.A, are shown by vertical dashed lines.

et al. [11], the long-time limit was not achieved. The populations of the states as a function of exposure time to π-polarized optical fields of various strengths are shown in Fig. 1. As shown in Section 2.A, the time for an atom with the mean kinetic energy to cross to the midpoint of the beam is 186 ns which is marked in Fig. 1. Due to the rapid transit time, the optical pumping process is far from complete. Moreover, the optical pumping process is less complete for a smaller field. This observation, combined with unexplained rapid rise in the Kerr coefficient at low optical power shown in Fig. 2(a), motivated the present study.

2. THEORY

The susceptibility χ is related to the polarization P by

$$P = \epsilon_0 \chi E, \tag{4}$$

where ϵ_0 is the permittivity of free space, and E is the electric field. For a medium for which Clausius–Mossotti local-field effects are negligible, the polarization is also given by

$$P = n_{\mathrm{den}} q_e \mathrm{Tr}(\mathbf{r}\sigma), \tag{5}$$

where n_{den} is the number density of atoms in the medium, q_e is the charge on the electron, $\mathbf{r}$ is the dipole operator, and σ is the density matrix written within the rotating wave approximation (RWA) to remove the optical carrier frequency. Equations (4) and (5) can be combined to give χ in terms of σ for a specified electric field E and atomic system.

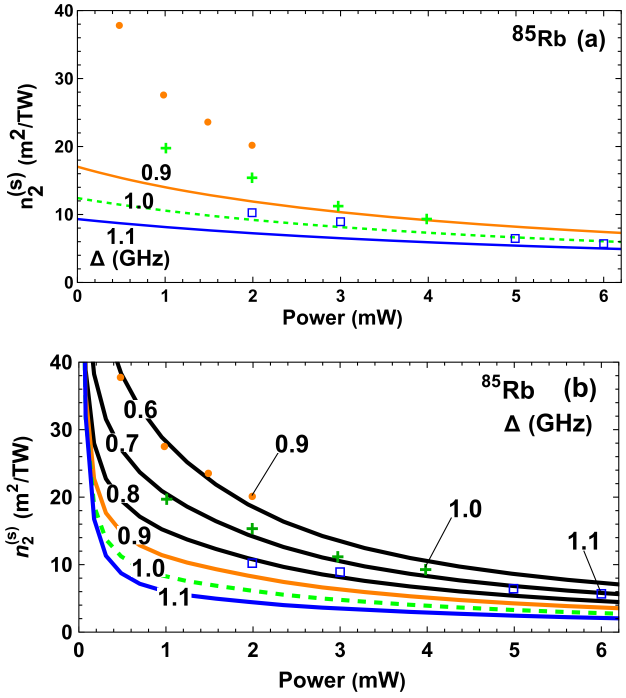

Fig. 2. The saturated Kerr coefficient of ^{85}Rb is shown. The data points in both subfigures are from the experiment of McCormick *et al.* [11] for blue detunings of 0.9 GHz (orange circles), 1.0 GHz (green crosses), and 1.1 GHz (blue squares). (a) Simplified reprint of Fig. 2a from Ref. [13]. The theory is for a two-level system and is given for detunings of 0.9 GHz (orange line), 1.0 GHz (dashed green line), and 1.1 GHz (blue line). (b) The present calculation is shown for detunings of 0.6–1.1 GHz. Lines are marked as in part (a) with the additional lines as marked in black. The experimental data are as in part (a).

In this work, the populations and coherences of each magnetic sublevel as a function of time were calculated by propagating the density matrix in an optical field with a fixed amplitude. The Lindblad master equation for the density matrix σ is

$$\frac{d\sigma}{dt} = -i[H, \sigma] + \left.\frac{d\sigma}{dt}\right|_{\mathrm{relax}}, \tag{6}$$

where H is the Hamiltonian and $\frac{d\sigma}{dt}|_{\mathrm{relax}}$ describes the relaxation. The relaxation is assumed to be due to spontaneous emission. Initially, the density matrix is set so that each magnetic sublevel of the ground states is equally populated, there is no excited state population, and there are no correlations. Hence, the off-diagonal elements of $\sigma(0)$ are 0.

The previous paper [13] primarily presented analytical results from a two-level system, although some results were based on the long-time density matrix propagation of a four-level system. The two-level system results themselves were derived from a density-matrix formulation taken in the long-time limit [12]. The present paper relies on the solution method of the density matrix as given in Appendix B of the previous paper with one exception. Both papers propagate the density matrix in time using

$$\sigma(t+\delta t)=\exp(\mathcal{L}\delta t)\sigma(t), \quad (7)$$

assuming the Lindblad matrix $\mathcal{L}$, specified in the previous paper [13], is constant throughout the time step δt. Whereas, in the previous paper Eq. (7) was implemented in Fortran with Horner's method, here Eq. (7) is implemented with sparse matrix methods using the Mathematica's MatrixExp function. Various methods for computing the matrix exponential are the subject of a review article [14].

Although the solution method is the same as in the previous paper, the systems used earlier averaged over the magnetic sublevels, and therefore are not capable of describing incomplete optical pumping as shown in Fig. 1. The present theory implements the density matrix with all magnetic sublevels. On its face, this involves large matrices. If there are $N_{\text{tot}}=N_{\text{gnd}}+N_{\text{exc}}$ states, where N_{tot} is the total number of states, N_{gnd} is the number of ground states, and N_{exc} is the number of excited states, the Lindblad matrix has N_{tot}^4 elements, but only $O(N_{\text{tot}}^2)$ of these are non-zero if the Hamiltonian has dipole selection rules and the relaxation matrix is due to spontaneous emission.

For the D2 line, $N_{\text{gnd}}=12$ and $N_{\text{exc}}=24$ for ^{85}Rb and $N_{\text{gnd}}=8$ and $N_{\text{exc}}=16$ for ^{87}Rb. The density matrix is thus 36 × 36 or 24 × 24 for the two cases, and the Lindblad matrix is 1296 × 1296 or 576 × 576, respectively. Because over 99% of the Lindblad matrix elements are zero, sparse matrix techniques are highly effective. In practical terms, all of the computational results presented in this paper combined were run in a few hours on a workstation using Mathematica 13.1.

One additional benefit of working with all of the magnetic sublevels is that the Hamiltonian may be defined with empirical parameters, including a reduced matrix element, a lifetime, and energy levels, all of which have been curated [15,16]. In the previous paper, which worked with hyperfine levels but not their magnetic sublevels, it was necessary to assume a sign of one of the matrix elements. Here, all the signs are given by the theory of angular momentum, with both formulas and explicit values given by Steck [15,16].

The dipole matrix elements associated with $\mathbf{r}$ depend on a single reduced matrix element and coefficients derived by angular momentum theory, given in detail by Steck [15,16]. The formulas are analogous to the Wigner–Eckart theorem, but the Clebsch–Gordan coefficients are replaced by a more complicated angular momentum coupling. These elements enter the Hamiltonian through the $\mathbf{E}\cdot\mathbf{r}$ interaction and also through the dipole moment operator $\mathbf{r}$ in the trace in Eq. (5). The formulas used here are given in the Appendix A.

A. Velocity Distribution and Averaging

Given the short transit time of the beam, the saturated polarizability depends on the history of the atoms. The magnitude of the saturated Kerr coefficient varies over time. Hence, the Kerr coefficient was varied over the velocity distribution of the atoms to capture this effect as well as the longitudinal Doppler effect.

Without a buffer gas, hot rubidium atoms tend not to interact with each other. The laser field is too weak to lead to significant forces on the hot atoms. Hence, the velocity of the atoms obeys the Maxwell distribution. By the equipartition theorem, the average kinetic energy in each direction is $\frac{1}{2}k_B T$, where k_B is the Boltzmann constant. An atom whose kinetic energy of 1D motion corresponds to the mean value obeys

$$\frac{1}{2}k_B T=\frac{1}{2}mv^2, \quad (8)$$

which may be solved for the velocity v. The quantity m is the mass of the atom. As an example, the temperature T in the experiment of McCormick *et al.* [11] is $T=78^\circ\text{C}=351$ K. If the mass of the atom corresponds to the average mass of ^{85}Rb and ^{87}Rb or 86 u, then $v=183$ m/s. The Rayleigh length z_R is given as 6 mm [11]. The wavelength λ of the Rb D2 transition is 780 nm, so the beam waist $w_0=39$ μm using

$$z_R=\frac{\pi w_0^2}{\lambda}. \quad (9)$$

The time of exposure t to an equivalent constant electric field may be estimated taking the Gaussian electric field

$$E(x)=E_0\, e^{-\frac{x^2}{w_0^2}}, \quad (10)$$

and a uniform velocity $x=vt'$,

$$E_0 t=E_0\int_{-\infty}^{0}\mathrm{d}t'\, e^{-\left(\frac{vt'}{w_0}\right)^2}. \quad (11)$$

The integral is well known, leading to

$$t=\frac{\sqrt{\pi}w_0}{2v}. \quad (12)$$

At the mean velocity, the time is 186 ns. In the calculation, a constant field is applied for simplicity. The time given in Eq. (12) yields the same time-electric field area as an atom passing at the same velocity would have going from infinity to the center of the beam.

Both transverse and longitudinal averaging of the thermal distribution were performed for the results shown in Figs. 2 and 3. The Maxwell distribution is separable. That is, the Maxwell probability density

$$f_M(v_x,v_y,v_z)=f_M^{(1)}(v_x)f_M^{(1)}(v_y)f_M^{(1)}(v_z) \quad (13)$$

with

$$f_M^{(1)}(v_i)=\left(\frac{m}{2\pi k_B T}\right)^{1/2}\exp\left(-\frac{mv_i^2}{2k_B T}\right), \quad (14)$$

where $f_M^{(1)}(v_i)$ is the 1D Maxwell distribution, m is the mass of the atom, k_B is the Boltzmann constant, and T is the temperature.

To average over the time an atom spends in the beam, only the transverse velocity distribution is needed, under the assumptions that particles traverse the beam through the focal region and that the interaction region is small compared to the Rayleigh length. In this case, the beam is approximately translationally invariant. The effect of transverse averaging is treated approximately by averaging over the time it takes for an atom to reach the beam center, where the time is given by Eq. (12) and the

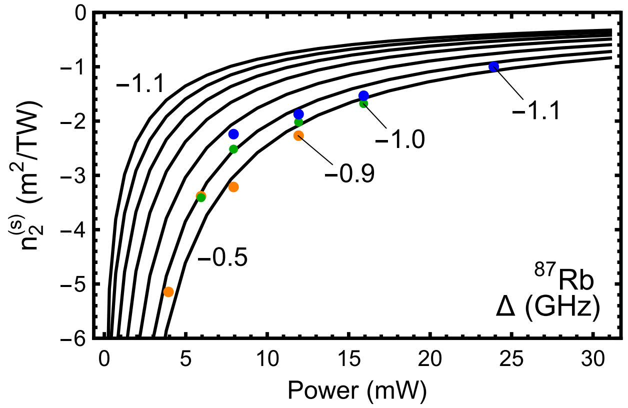

Fig. 3. The saturated Kerr coefficient is given for the experiment of McCormick *et al.* [11] −0.9 GHz (orange circles), −1.0 GHz (green crosses), and −1.1 GHz (blue squares) for ^{87}Rb and compared to theoretical calculations with Δ from −0.5 to −1.1 GHz in 0.1 GHz intervals. One of the experimental points at −1.0 GHz is nearly equal to another experimental point at −0.9 GHz.

velocity distribution is given by Eq. (14) restricted to positive velocities. As noted above, the field is taken as a constant. The calculation was performed for 41 times between 10 ns and 100 μs, equally spaced in the logarithm of the time.

To average over the Doppler broadening, only the longitudinal velocity distribution appears. The atoms are moving slowly compared to the speed of light: $v/c \approx 10^{-6}$. To first order in v/c, there is no transverse Doppler effect and the longitudinal frequency shift is $\omega_0 v/c$, where ω_0 is the optical transition frequency. The Doppler shift is treated by convolving the 1D Maxwell distribution with a standard deviation of about 230 MHz with the results obtained for various values of the detuning. The detuning was found for 29 values of the detuning Δ from ±0.1 to ±1.5 GHz in steps of 0.05 GHz, where the positive sign (blue detuning) is taken for ^{85}Rb and the negative sign (red detuning) for ^{87}Rb. The convolution was performed with a Gaussian weighting on 17 equally spaced values of the detuning.

Separate calculations were performed for 20 electric field values, either from 2.5 to 50 kV/m for ^{85}Rb or 5 to 100 kV/m for ^{87}Rb to have solutions for the various power levels given in Figs. 2 and 3. In total, the Lindblad master equation, Eq. (6), was solved $2 \times 20 \times 29 = 1160$ times, with 41 time points in each solution for the results presented in this work.

3. RESULTS

The results of the calculation are given in Fig. 2 for ^{85}Rb and Fig. 3 for ^{87}Rb. As in Fig. 1, π polarization is assumed. The theoretical results are compared to the experiment of McCormick *et al.* [11]. The independent variable "power" follows the convention of the experiment. Conversion formulas are given in our earlier paper [13]. The electric field of 10 kV/m corresponds to a power of 0.31 mW and the field of 50 kV/m corresponds to a power of 7.8 mW.

The calculation is presented at the experimental values of the detuning, namely ±0.9 GHz, ±1.0 GHz, and ±1.1 GHz for ^{85}Rb and ^{87}Rb. For these values, there is semiquantitative agreement with the experiment. The rapid variation at low power and the shifts from one value of detuning to another display the trends of the experiment. The calculation was extended to three additional detunings to illustrate the possibility of better agreement if a free parameter is allowed. Specifically, there is a shift of −0.3 GHz for ^{85}Rb and +0.4 GHz for ^{87}Rb. The present theory predicts a little more variation than is found experimentally. The differences in $n_2^{(s)}$ for a 0.1 GHz step are in good agreement for ^{85}Rb, but are too large for ^{87}Rb.

Previously published results based on a two-level system are shown in Fig. 2(a). The two-level theory gives a fair account of the experimental data at high power, but does not capture the dramatic rise at low power present for the detuning of 0.9 GHz and, to a lesser extent, 1.0 GHz. In contrast, the multi-level calculation including the effect of incomplete optical pumping does show this rise. At high power, the present results fall off faster than the two-level system results, being about three times smaller at 6 mW at the nominal detuning, leading to worse agreement with the experiment in this regime.

The adjustment of −0.3 GHz from the experiment to the present theory for ^{85}Rb and 0.4 GHz ^{87}Rb has no clear justification. Possibly the reference frequencies are not identical from the present theory to the experiment. The conversion from electric field strength to power depends on the Rayleigh length [13] which is only quoted to one significant digit in the experiment. Similarly, the absolute scale depends on the density which is quoted as 1.0×10^{18} m^{-3}, i.e., with up to 5% uncertainty due to truncation alone. The experimental data itself may have systematic errors due to using the Z-scan method [17,18] outside of its range of validity [10].

On the theoretical side, the constant-field approximation could be revisited, since the atoms see a field which varies as a Gaussian as the atoms pass through the beam. There is also an assumption that the atoms can be described by a single pass through the beam. Perhaps they do not relax to the assumed state of equally populated ground-state magnetic sublevels independent of the value of the angular momentum F after collisions with each other or the container.

4. CONCLUSIONS

In summary, I calculated the saturated Kerr coefficient in rubidium vapor taking into account incomplete optical pumping due to the finite transit time of the atoms through the laser beam, a common occurrence in experiments. There is a thermal average over both transverse and longitudinal components of the atoms' velocities. The density-matrix-based calculation includes all magnetic sublevels which is necessary because there is not enough time to complete optical pumping for the majority of the atoms crossing the beam. Although on its face the calculation involves forming the Lindblad matrix that scales as the fourth power of the number of atomic states in the calculation, in fact the sparsity of the Lindblad matrix for an electric dipole-interaction Hamiltonian reduces the scaling to the second power.

The new calculation captures the rapid changes in the saturated Kerr coefficients at low intensities leading to semiquantitative agreement with an experiment [11]. The previous calculation that does not include the effect of the finite transit time of the atoms does not show the rapid increase in the Kerr coefficient at low optical power. Further progress depends on both more detailed modeling as well as an improved experiment, as proposed earlier [10].

The concept of "the susceptibility of rubidium in a vapor cell" may need to be revisited. Usually, the optical susceptibility is calculated assuming the density matrix has reached an asymptotic value [12]. However, that is not the case in a representative experiment [11] or in a more recent demonstration of a rubidium-based frequency standard in a photonic cavity [19]. Moreover, Wang *et al.* [20] reported the Kerr coefficients for pulsed light in ^{87}Rb to be significantly higher than the values with a constant optical intensity. The susceptibility may depend on the history of the atoms in a more nuanced way than is typically recognized.

APPENDIX A: ANGULAR MOMENTUM FORMULAS

Steck's formulas [16] were used to find dipole matrix elements. The Hamiltonian requires the dipole matrix elements given by Steck's Eq. (34), namely

$$\langle F m_F | e r_q | F' m'_F \rangle = \langle F || e\mathbf{r} || F' \rangle \langle F m_F | F' m'_F ; 1 q \rangle, \quad \textbf{(A1)}$$

where F is the angular momentum of the hyperfine state, m_F is the azimuthal quantum number, e is the elementary charge, and r_q is a component of the dipole moment in the spherical basis. The primed quantities have similar definitions. The final matrix element is the Clebsch–Gordan coefficient. For π polarization, $q = 0$.

The reduced matrix element is given by Steck's Eq. (36):

$$\langle F || e\mathbf{r} || F' \rangle = \langle J || e\mathbf{r} || J' \rangle (-1)^{F'+J+1+I} \sqrt{(2F'+1)(2J+1)} \times \begin{Bmatrix} J & J' & 1 \\ F' & F & I \end{Bmatrix}. \quad \textbf{(A2)}$$

Here, I is the nuclear angular momentum, which is 5/2 for ^{85}Rb and 3/2 for ^{87}Rb, and the array is a 6-j symbol. The reduced matrix element for the combined electron spin and orbital angular momentum, $\langle J || e\mathbf{r} || J' \rangle$, is a property of the atomic transition and is tabulated [15,16]. The Clebsch–Gordan coefficients and the Wigner 6-j symbols are implemented in Mathematica 13.1. The angular factors in the matrix elements are also tabulated by Steck.

Funding. National Institute of Standards and Technology (NIST) Scientific and Technical Research and Services.

Disclosures. The author declares no conflicts of interest. The mention of a commercial product does not imply endorsement by the author's institution.

Data availability. The code which generated the theoretical results is available from the author upon reasonable request.

REFERENCES

1. D. E. Chang, V. Vuletić, and M. D. Lukin, "Quantum nonlinear optics-photon by photon," Nat. Photonics **8**, 685–694 (2014).
2. A. Dutt, A. Mohanty, A. L. Gaeta, *et al.*, "Nonlinear and quantum photonics using integrated optical materials," Nat. Rev. Mater. **9**, 321–346 (2024).
3. L.-A. Wu, H. Kimble, J. Hall, *et al.*, "Generation of squeezed states by parametric down conversion," Phys. Rev. Lett. **57**, 2520 (1986).
4. S. E. Harris, J. Field, and A. Imamoğlu, "Nonlinear optical processes using electromagnetically induced transparency," Phys. Rev. Lett. **64**, 1107 (1990).
5. U. Gaubatz, P. Rudecki, S. Schiemann, *et al.*, "Population transfer between molecular vibrational levels by stimulated Raman scattering with partially overlapping laser fields," J. Chem. Phys. **92**, 5363–5376 (1990).
6. G. Steinmeyer, D. Sutter, L. Gallmann, *et al.*, "Frontiers in ultrashort pulse generation: pushing the limits in linear and nonlinear optics," Science **286**, 1507–1512 (1999).
7. M. Lukin, P. Hemmer, and M. O. Scully, "Resonant nonlinear optics in phase-coherent media," Adv. At. Mol. Opt. Phys. **42**, 347–386 (2000).
8. A. Joshi and M. Xiao, "Controlling nonlinear optical processes in multi-level atomic systems," Prog. Opt. **49**, 97–175 (2006).
9. Z. L. Newman, V. Maurice, T. Drake, *et al.*, "Architecture for the photonic integration of an optical atomic clock," Optica **6**, 680–685 (2019).
10. Z. H. Levine, "Proposed experiment to measure nonlinear optical susceptibilities in the saturated regime," Phys. Rev. A **110**, 023501 (2024).
11. C. F. McCormick, D. R. Solli, R. Y. Chiao, *et al.*, "Saturable nonlinear refraction in hot atomic vapor," Phys. Rev. A **69**, 023804 (2004).
12. G. Grynberg, A. Aspect, and C. Fabre, *Introduction to Quantum Optics: from the Semi-Classical Approach to Quantized Light* (Cambridge University Press, 2010).
13. Z. H. Levine and Z. Du, "Semiclassical calculation of the power saturation of the Kerr effect in Rb vapor," J. Opt. Soc. Am. B **40**, 3190–3195 (2023).
14. I. Leonard, "The matrix exponential," SIAM Rev. **38**, 507–512 (1996).
15. D. A. Steck, "Rubidium 87 D line data" (2008), https://steck.us/alkalidata/rubidium87numbers.pdf.
16. D. A. Steck, "Rubidium 85 D line data" (2008), https://steck.us/alkalidata/rubidium85numbers.pdf.
17. M. Sheik-Bahae, A. A. Said, and E. W. Van Stryland, "High-sensitivity, single-beam n_2 measurements," Opt. Lett. **14**, 955–957 (1989).
18. M. Sheik-Bahae, A. A. Said, T.-H. Wei, *et al.*, "Sensitive measurement of optical nonlinearities using a single beam," IEEE J. Quantum Electron. **26**, 760–769 (1990).
19. M. T. Hummon, S. Kang, D. G. Bopp, *et al.*, "Photonic chip for laser stabilization to an atomic vapor with 10^{-11} instability," Optica **5**, 443–449 (2018).
20. S. Wang, J. Yuan, L. Wang, *et al.*, "Measurement of the Kerr nonlinear refractive index of the Rb vapor based on an optical frequency comb using the z-scan method," Opt. Express **28**, 38334–38342 (2020).

129.6.28.11 2025-05-23 12:06:05